Niclosamide Inhibits Oxaliplatin Neurotoxicity while Improving Colorectal Cancer Therapeutic Response

Olivier Cerles, Evelyne Benoit, Christiane Chéreau, Sandrine Chouzenoux, Florence Morin, Marie-Anne Guillaumot, Romain Coriat, Niloufar Kavian, Thomas Loussier, Pietro Santulli, et al.

Molecular Cancer Therapeutics

Niclosamide Inhibits Oxaliplatin Neurotoxicity while Improving Colorectal Cancer Therapeutic Response

Olivier Cerles[1], Evelyne Benoit[2,3], Christiane Chéreau[1], Sandrine Chouzenoux[1], Florence Morin[1,4], Marie-Anne Guillaumot[1,5], Romain Coriat[1,5], Niloufar Kavian[1,4], Thomas Loussier[1], Pietro Santulli[1,6], Louis Marcellin[1,6], Nathaniel E.B. Saidu[1], Bernard Weill[1,4], Frédéric Batteux[1,4], and Carole Nicco[1]

Abstract

Neuropathic pain is a limiting factor of platinum-based chemotherapies. We sought to investigate the neuroprotective potential of niclosamide in peripheral neuropathies induced by oxaliplatin. Normal neuron-like and cancer cells were treated *in vitro* with oxaliplatin associated or not with an inhibitor of STAT3 and NF-κB, niclosamide. Cell production of reactive oxygen species and viability were measured by 2′,7′-dichlorodihydrofluorescein diacetate and crystal violet. Peripheral neuropathies were induced in mice by oxaliplatin with or without niclosamide. Neurologic functions were assessed by behavioral and electrophysiologic tests, intraepidermal innervation, and myelination by immunohistochemical, histologic, and morphologic studies using confocal microscopy. Efficacy on tumor growth was assessed in mice grafted with CT26 colon cancer cells. In neuron-like cells, niclosamide downregulated the production of oxaliplatin-mediated H_2O_2, thereby preventing cell death. In colon cancer cells, niclosamide enhanced oxaliplatin-mediated cell death through increased H_2O_2 production. These observations were explained by inherent lower basal levels of GSH in cancer cells compared with normal and neuron-like cells. In neuropathic mice, niclosamide prevented tactile hypoesthesia and thermal hyperalgesia and abrogated membrane hyperexcitability. The teniacide also prevented intraepidermal nerve fiber density reduction and demyelination in oxaliplatin mice in this mixed form of peripheral neuropathy. Niclosamide prevents oxaliplatin-induced increased levels of IL6, TNFα, and advanced oxidized protein products. Niclosamide displayed antitumor effects while not abrogating oxaliplatin efficacy. These results indicate that niclosamide exerts its neuroprotection both *in vitro* and *in vivo* by limiting oxaliplatin-induced oxidative stress and neuroinflammation. These findings identify niclosamide as a promising therapeutic adjunct to oxaliplatin chemotherapy. *Mol Cancer Ther; 16(2); 300–11. ©2016 AACR.*

Introduction

Platinum-based chemotherapies elicit their antitumor effects by compromising the integrity of DNA via the formation of adducts and impairing the functioning of mitochondrial processes (1–3). These impairments ultimately lead to a burst of oxidative stress, which in turn promotes cell death processes (4). Oxaliplatin is able to induce functional abnormalities in dorsal root ganglia and axonal voltage-gated sodium channels as well as voltage-gated potassium channels (5–7). Oxaliplatin also induces a deregulation in calcium intracellular signaling as well as homeostasis (8, 9). This platinum-based chemotherapy indicated in metastatic colon cancers and colorectal cancers has also been shown to induce a rise in tumor cell production of reactive oxygen species (ROS; ref. 10). Oxaliplatin is indicated as a first-line and an adjuvant treatment. This molecule is associated with several toxicities, such as a high risk for allergic reactions, hepatotoxicity, and peripheral neuropathies that affect up to 95% of patients (11). Oxidative stress is a key factor in the induction of oxaliplatin-associated peripheral neuropathies (1, 12, 13). This oxidative stress has also been linked to transient receptor potential cation channel TRPA1, which acts as a sensor of electrophilic and reactive species generated during tissue injury and inflammation (14). It is thought that by-products generated by ROS following oxaliplatin treatment could activate TRP1A, thereby producing a nociceptive response and neurogenic inflammation (15). Furthermore, antioxidant molecules, such as vitamin C, acetyl-L-carnitine, and α-linoleic acid, can inhibit ROS-induced hyperalgesia in rats presenting peripheral neuropathies induced by oxaliplatin, via IB4-positive nociceptors (16). This observation concurs with the fact that oxaliplatin can modulate sodium channel activity, thereby influencing the sensitivity of nociceptors (17). Oxaliplatin neurotoxicity may manifest within hours after injection as an acute reaction or as a chronic response

[1]Department "Development, Reproduction and Cancer", Institut Cochin, Paris Descartes University, Sorbonne Paris Cité, INSERM U1016, Paris, France. [2]Institut des Neurosciences Paris-Saclay, UMR 9197, CNRS, Gif-sur-Yvette, France. [3]Molecular Engineering of Proteins Unit (DRF/iBiTec-S/SIMOPRO), CEA of Saclay, Gif-sur-Yvette, France. [4]Department of Immunology, Cochin Teaching Hospital, AP-HP, Paris, France. [5]Department of Gastroenterology, Cochin Teaching Hospital, Paris Descartes University, Paris, France. [6]Department of Gynecology Obstetrics II and Reproductive Medicine, Cochin Teaching Hospital, Paris, France.

Note: Supplementary data for this article are available at Molecular Cancer Therapeutics Online (http://mct.aacrjournals.org/).

F. Batteux and C. Nicco contributed equally to this article.

Corresponding Author: Frédéric Batteux, Institut Cochin, Paris Descartes University, Sorbonne Paris Cité, INSERM U1016, 8, rue Méchain, Pav Gustave Roussy, Paris 75679, France. Phone: 336-6065-5279; Fax: 331-5841-2008; E-mail: frederic.batteux@cch.aphp.fr

doi: 10.1158/1535-7163.MCT-16-0326

AACR

resulting from cumulated high-dosage injections. The acute form, which is reversible and usually resolves within days following injection, is characterized by transient paresthesia and myotonia, whereas the chronic form presents persistent paresthesia and thermoalgesia (18). This toxicity may require lowering of doses and, in worst cases, interruption of the treatment (19). Targeting the pathogenic events leading to the oxidative burst witnessed upon injection of oxaliplatin may prove useful in preventing neurotoxicity.

Niclosamide is an antihelminthic drug with a well-known safety profile. This drug is known for its inhibitory effects on oxidative phosphorylating activity and for its anti-inflammatory properties. Niclosamide also exhibits antitumor effects through the inhibition of pathways commonly associated with oncogenesis, such as STAT3, NF-κB, Wnt/β-catenin, mTORC1, and Notch (20). Niclosamide sensitizes cancer cells that are nonresponsive to radiotherapy (21), and *in vitro* potentiation of the antitumor effects of chemotherapeutics upon association with niclosamide has been reported (22).

The anti-inflammatory properties of niclosamide prompted us to investigate *in vitro* and *in vivo* its protective potential in both preventing the neurologic impairments brought about by oxaliplatin, as well as enhancing its antitumor effect.

Materials and Methods

Cell culture and treatments

All cell lines were authenticated by short tandem repeat analysis and tested negative for mycoplasma in April 2014. CT26 (mouse colon carcinoma) cells, purchased from the ATCC in 2012, were grown in DMEM with 10% FBS, penicillin/streptomycin, and L-glutamine supplementation. N2a (mouse brain neuroblastoma) cells, purchased from the ATCC in 2012, were grown in Eagle Minimum Essential Medium supplemented with 10% FBS, penicillin/streptomycin, 2% sodium pyruvate, 1% ciprofloxacin, nonessential amino acids, and L-glutamine supplementation. HUVECs (human umbilical vein endothelium), purchased from the ATCC in 2012, were grown in endothelial cell basal medium-2 with 10% FBS, 1% ciprofloxacin, penicillin/streptomycin, and essential amino acids. THP1 (human acute leukemia monocyte) cells, purchased from the ATCC in 2012, were grown in RPMI medium 1640 with 10% FBS and penicillin/streptomycin.

ROS, GSH, and viability assays

All cells (1.5×10^4–10^5 per well) were seeded in 96-well plates (Corning) and incubated for 16 hours with 0.05 μmol/L of niclosamide (Sigma-Aldrich) and treated with 0 to 50 μmol/L of oxaliplatin (Accord Healthcare Limited). Cell viability was assessed by crystal violet assay, and results are expressed as the mean percentage of viable cells ± SD versus cells not exposed to oxaliplatin (100% viability). Cellular production of hydrogen peroxide (H_2O_2) and reduced glutathione (GSH) was assessed by spectrofluorimetry with 2′,7′-dichlorodihydrofluorescein diacetate and monochlorobimane, respectively (10).

Drug treatment study

BALB/cJRj male mice between 6 and 8 weeks of age were purchased (Janvier Labs). If not explicitly stated otherwise, mice received intraperitoneal injections (200 μL) of first, either oxaliplatin (10 mg/kg; ref. 23) or vehicle alone each Monday and second, either niclosamide (10 mg/kg) or vehicle alone each Monday (6 hours after the first injection; ref. 1), Wednesday, and Friday, for 4 to 8 weeks. All animals were kept in identical housing conditions and euthanized by cervical dislocation preceded by isoflurane inhalation. Animals received humane care in compliance with French Institutional Guidelines (INSERM and Université Paris Descartes – Ethics Committee CEEA 34).

Behavioral studies

Tactile sensitivity was evaluated using the von Frey test. The principle of this test is standardized: Once the mouse is calm and motionless, a hind paw is touched with the tip of a flexible fiber of given length and diameter. The fiber is pressed against the plantar surface at a right angle and exerts a vertical force. The force of application increases as long as the investigator is pushing the probe and until the fiber bends. This principle makes it possible for the investigator to apply a reproducible force to the skin surface. The scale of force used ranged from 0.008 to 0.400 g. The von Frey test was considered positive when the animal indicated a perception of the fiber by pulling back its paw (24). Paw movements associated with locomotion were not counted as a withdrawal response. Cold hyperalgesia was evaluated using the protocol described by Ta and colleagues (25). Mice were treated daily with oxaliplatin (3 mg/kg) or vehicle for 5 days, followed by 5 days of rest, for 2 cycles. Hyperalgesia was evaluated by the cold plate assay at the optimal temperature of 2°C ± 0.2°C as described previously (1, 25). The total number of brisk lifts of one or the other hind paw was counted as the response to cold hyperalgesia, and two observers were tasked with counting to ensure accuracy. Normal locomotion was distinct, involving coordinated movements of all four limbs that were excluded. A maximal cut-off time of 5 minutes was used to prevent tissue damage. A cold plate test was performed at baseline, during, and after drug treatment at the end of each of the two cycles over the 5-day period. Results are expressed as the mean ± SD of the observers' counts.

Electrophysiologic exploration of oxaliplatin neurotoxicity

The sensory and motor excitability was assessed *in vivo* on mice under isoflurane (AErrane) anesthesia by minimally invasive electrophysiologic methods using the Qtrac software written by Prof. H. Bostock (Institute of Neurology, London, United Kingdom), as described previously (26). Briefly, an anaesthetized mouse was placed on a heating pad to the maintain body temperature throughout the experiment (between 35.40 ± 0.04 and 35.47 ± 0.02°C, as determined in 29 mice using a rectal probe) to avoid nonspecific modifications of the measured excitability parameters. For sensory investigation, the compound nerve action potential (CNAP) was recorded using needle electrodes inserted into the base of mouse tail, in response to stimulation of the caudal nerve applied at the distal part of the tail, by means of surface electrodes. For motor investigation, electrical stimulation was delivered to the sciatic motor nerve, and the compound muscle action potential (CMAP) was recorded into the plantar muscle. The mouse was systematically submitted to the first session of excitability measurements (TRONDE protocol), allowing to determine the stimulus–response relationship (i.e., the CNAP or CMAP amplitude as a function of 1-ms stimulation intensity), and thus evaluate notably the CNAP or CMAP maximal amplitude, the stimulation intensity that had to be applied to

evoke a CNAP or CMAP of 50% maximal amplitude, and the latency measured from stimulation onset to peak amplitude, giving information on the global excitability state. For motor recordings, this first excitability test was followed by four different other ones performed together: (i) the strength–duration relationship (i.e., the intensity in relation to the duration of a stimulus necessary to evoke a given amplitude of CMAP), which evaluated the minimal intensity of infinitely long duration stimulation necessary to evoke a CMAP (rheobase) and the intensity duration of twice the rheobase stimulation necessary to evoke a CMAP (chronaxie), giving information on the axonal resting potential at the nodal membrane; (ii) the current–threshold relationship (i.e., the threshold changes at the end of 200-ms conditioning subthreshold depolarizing and hyperpolarizing currents ranging from 50% to 100% thresholds); (iii) the threshold electrotonus (i.e., the threshold changes during and after 100-ms conditioning subthreshold depolarizing and hyperpolarizing currents applied at ±40% thresholds), which evaluates the electrotonic changes in membrane potential, giving information on axonal accommodation capacities to depolarizations and hyperpolarizations; and (iv) the recovery cycle (i.e., the excitability changes that occur following a CMAP), which evaluated the refractory periods (during which membrane excitability is either nil or markedly decreased) followed by the supernormal and late subnormal periods (during which membrane excitability is increased and decreased, respectively). As a whole, more than 30 parameters could be determined from these excitability tests and analyzed. It is worth noting that each specific excitability test provides additional and complementary information regarding, on one hand, the functional status of ion channels and electrogenic pumps and, on the other hand, membrane properties (27, 28).

Confocal microscopy

The experiments were carried out on single myelinated axons isolated from the sciatic nerves, as detailed previously (29). Briefly, sciatic nerve sections of about 2 cm in length were removed from their sheaths, dissected, and fixed for 1 hour in PBS (1×) with 2% PFA, then rinsed three times with PBS (1×). Sciatic nerves were deposited on microscope slides, myelinated axons were gently teased apart from the main trunk, and preparations were kept at −20°C until use. Just before the experiments, sciatic nerves were rehydrated for about 1 hour with a standard physiologic solution containing 154 mmol/L NaCl, 5 mmol/L KCl, 2 mmol/L $CaCl_2$, 1 mmol/L $MgCl_2$, 11 mmol/L glucose, and 5 mmol/L HEPES, buffered at pH 7.4 with NaOH. Preparations were then exposed for 30 minutes to the fluorescent dye FM1-43 (Molecular Probes) dissolved in a standard physiologic solution to stain the plasma membranes of the myelinated axons and washed with dye-free solution before imaging. A Zeiss LSM 510 META (Carl Zeiss) multiphoton scanning confocal microscope, mounted on an upright microscope and controlled with the manufacturer's software and workstation, was used for optical sectioning of myelinated axons and subsequent 3D high-resolution digital reconstruction of their structure. Images were collected using a 63× oil immersion objective with a 1.40 numerical aperture (Zeiss Plan-Apochromat), following excitation of FM1-43 with the 488-nm wavelength line of an Argon ion laser, and then digitized at 12-bit resolution into a 512 × 512 pixel array. Images were then analyzed using ImageJ software (NIH, Bethesda, MD). Quantification of morphometric parameters of myelinated axons was performed by measuring the internodal diameter, nodal diameter (D) and nodal length (L). Assuming the simplest geometry in which a node of Ranvier approaches a cylinder, the nodal volume (V) was then determined as $V = \pi L\ (D/2)^2$.

IHC and histology

Intraepidermal nerve fibers density and myelin sheath of sciatic nerves were evaluated by IHC and histology. Luxol Blue Fast allows for fast, reliable, and reproducible staining of myelin in transversal section of sciatic nerves (30–32). Briefly, sciatic nerves were removed and preserved in formol before being fixed in paraffin and stained with coloring solution (Luxol Blue Fast Solution). Sections of skin from the hind paws of mice were preserved in buffered 4% formol (VWR Chemicals, Labonord SAS) and immersed in successive baths of increasing concentration of ethanol (50%, 70%, 90%, and 100%). Samples were then immersed in xylene substitute before being fixed in paraffin, kept at 4°C, and cut into 6-μm thick slices. Samples were then dewaxed in three successive baths of xylene substitute for 3 minutes and rehydrated in ethanol baths for 1 minute each, starting with two baths of pure ethanol followed with baths of 90%, 70%, and 30% ethanol and two baths of H_2O. Slides were then washed in PBS for 2 minutes before being immersed in citrate buffer at 95°C for 10 minutes. Samples were then washed in three baths of PBS of 5 minutes each. Samples were then permeabilized [PBS, Triton X-100 (0.25%)] for 10 minutes before being rinsed in PBS in three baths of 5 minutes each and immersed in a blocking solution (PBST, 10% goat serum, 1% BSA) for at least 180 minutes. Samples were then incubated at 4°C overnight in the primary antibody (Abcam, ab10404, rabbit polyclonal to PGP9.5, 1:1,000) before being rinsed in PBS in three baths of 5 minutes each and incubated in the secondary antibody (Sigma, F9887, anti-rabbit IgG FITC-conjugate, 1:1,000) at room temperature in the dark. Prior to mounting (Thermo Scientific, Shandon Immu-Mount), slides were washed with PBS in three baths of 5 minutes each. Images were collected using a Nikon Eclipse 80i microscope with a Nikon Plan Fluor 100×/1.30 oil immersion DIC H/N2 objective.

Tumor growth

A total of 1×10^6 viable CT26 cells, as determined by Trypan blue staining and resuspended in DMEM, were then injected subcutaneously into the back of BALB/cJRj mice. When tumors reached a mean size of 200 to 500 mm^3, animals were randomized and received a single weekly injection of either oxaliplatin (10 mg/kg) or vehicle. At the same time, mice were injected or not with niclosamide (10 mg/kg) every day. Following randomization, tumor size was measured with a numeric caliper twice a week for 3 weeks. To comply with ethical guidelines, tumor growth experiments were stopped 3 weeks after the first oxaliplatin injection. Tumor volume was calculated as follows: $TV\ (mm^3) = (L \times W^2)/2$, where L is the longest and W the shortest radius of the tumor in millimeters. Results are expressed as means ± SD of tumor volumes ($n = 8$ in each group).

ELISA assays

Sera were retro-orbitally punctured 4 weeks after the first injection of oxaliplatin. Samples were diluted (1:4) in assay diluent 1× or ELISA/ELISPOT diluent 1× (the manufacturer's kits respective diluent solutions) before being distributed on

ELISA 96-well plates specific of IL6 and TNFα (Mouse IL-6 ELISA Ready-SET-Go! and Mouse TNF ELISA Ready-SET-Go!; eBioscience). Concentrations were calculated from a standard curve according to the manufacturer's protocol.

Advanced oxidized protein products assay

The level of oxidative stress was determined in all experimental mice groups as described previously (1). Prior to being dispensed into a 96-well plate (Corning), sera were diluted (1:4) in PBS. Acetic acid was then added to each well (20 μL). A standard curve was drawn after adding 10 μL 1.16 mol/L potassium iodide to 100 μL chloramine-T solution (0–100 μmol/L; Sigma-Aldrich) and 20 μL acetic acid. The blank was prepared similarly, but the chloramine-T solution was replaced by an equal volume of PBS. The absorbance was read immediately at 340 nm. The advanced oxidation protein products (AOPP) concentrations were expressed as micromoles per liter of chloramines-T equivalents (1).

Statistical analysis

Statistical analysis was performed using GraphPad Prism 5. Artwork was also created using GraphPad Prism 5, except for electrophysiologic study artwork, which was created using the Qtrac software. Differences between values were tested using the two-tailed Student *t* test, two-way ANOVA, or the nonparametric Mann–Whitney *U* test, depending on the equality of variances estimated using Lilliefors test. They were considered significant when $P < 0.05$. *P* values are denoted as follows: *, $P < 0.05$; **, $P < 0.01$; ***, $P < 0.001$; ****, $P < 0.0001$; NS, not significant.

Results

To assess the neuroprotective potential of niclosamide on oxaliplatin-induced peripheral neuropathies, we used a cellular model of the condition involving the exposition of neuron-like cells to both the chemotherapy and the teniacide. To further evaluate the therapeutic value of niclosamide, the efficacy of oxaliplatin when associated with the teniacide also had to be investigated, as niclosamide could have dampened the antitumor effect of the chemotherapy. Our results indicate that niclosamide modulated cell viability in a cell type–dependent manner. Niclosamide permitted a greater cytotoxicity of oxaliplatin on CT26 and THP1 cells (Fig. 1A and C). Inversely, in niclosamide-treated neuron-like N2a cells, the cytotoxicity of oxaliplatin was diminished (Fig. 1B). Niclosamide did not further increase oxaliplatin-mediated cell death of HUVECs (Fig. 1C). This cell type–dependent death was accompanied by a greater rise in H_2O_2 production (Fig. 1A and D), while protection of neuron-like cells was mediated by niclosamide through a significant decrease in H_2O_2 production (Fig. 1B). The innocuity of niclosamide on HUVECs that are analogous to the cells forming vasa nervorum *in vivo* is of prime importance as an *in vitro* deleterious effect of the teniacide might have reflected an *in vivo* reduction in blood flow supply to the peripheral nerves possibly leading to peripheral neuropathies. Cell type–dependent H_2O_2-mediated cell death was explained through differential basal levels of GSH (Fig. 1E). Indeed, N2a cells produce higher levels of GSH than CT26 under normal conditions, therefore allowing for greater cytotoxicity of niclosamide on the latter cell line when also incubated with oxaliplatin (Fig. 1A and B).

The aforementioned *in vitro* results suggested that, *in vivo*, niclosamide could potentially prevent neurologic alterations resulting from oxaliplatin infusions while potentiating their efficacy. To determine whether niclosamide could indeed abrogate the main limiting factor of oxaliplatin treatment, mice were subjected to neurologic tests similar to those used in patients treated by oxaliplatin. A von Frey test after 4 weeks of treatment showed that the withdrawal threshold was four times higher in mice treated with oxaliplatin than in mice treated with vehicle alone (Fig. 2A). Niclosamide corrected this hypoesthesia and permitted the maintenance of tactile sensitivity in mice also treated with oxaliplatin (Fig. 2A).

In addition to diminished tactile sensitivity, patients treated by oxaliplatin also suffer from altered thermal perception at their extremities, and mice models have been developed to mimic these neurologic disorders (5). After oxaliplatin cycle 1, the mean number of brisk lifts was four times higher in oxaliplatin mice than in mice injected with vehicle alone (Fig. 2B). The same changes were observed after the second cycle of treatment. Association with niclosamide rescued this hyperalgesia (Fig. 2B). Together, these data demonstrate *in vivo* a beneficial effect of niclosamide on key peripheral functions.

Oxaliplatin-treated mice presented significant alterations, consistent with membrane hyperexcitability, in excitability waveforms and derived parameters, compared with animals injected with vehicle alone. For sensory recordings (Fig. 3), these alterations consisted in (i) a decreased CNAP amplitude; (ii) a consequent enhanced latency, that is, a decreased nerve conduction velocity, suggesting apparent reduction in the number of fast-conducting fibers or decrease in density and/or functioning of nerve transitory sodium channels; and (iii) a reduced stimulus intensity to evoke 50% of maximal CNAP amplitude, indicating modification in the voltage dependence of these channels. For motor recordings (Supplementary Fig. S1; Supplementary Table S1), the alterations involved mainly (i) an enhanced CMAP amplitude and a reduced stimulus intensity to evoke 50% of maximal CMAP amplitude, suggesting apparent decreased density and/or functioning of fast potassium channels and modification in the voltage dependence of transitory sodium channels, respectively, with no change in the latency, that is, no modification in the neurotransmission velocity; (ii) reduced minimum and hyperpolarizing slopes of the current–threshold relationship, indicating decreased density and/or functioning of cyclic nucleotide-gated channels; (iii) increased threshold changes in response to hyperpolarizing currents (threshold electrotonus), likely caused by reduced inward rectifier potassium channels; and (iv) increased refractoriness and lower superexcitability (recovery cycle), reflecting again transitory sodium and fast potassium channel dysfunctioning, respectively. The absence of oxaliplatin-induced modification of strength–duration relationship (Supplementary Fig. S1) and threshold changes in response to depolarizing currents (Supplementary Fig. S1), and derived parameters (Supplementary Table S1), strongly suggests that the antitumor agent does not affect the density and/or functioning of persistent sodium channels and slow potassium channels, respectively, and thus does not produce any change in resting membrane potential. This latter conclusion is supported by the absence of oxaliplatin effect on parameters #24 (Supplementary Table S1; threshold electrotonus) and #14 (Supplementary Table S1; recovery cycle).

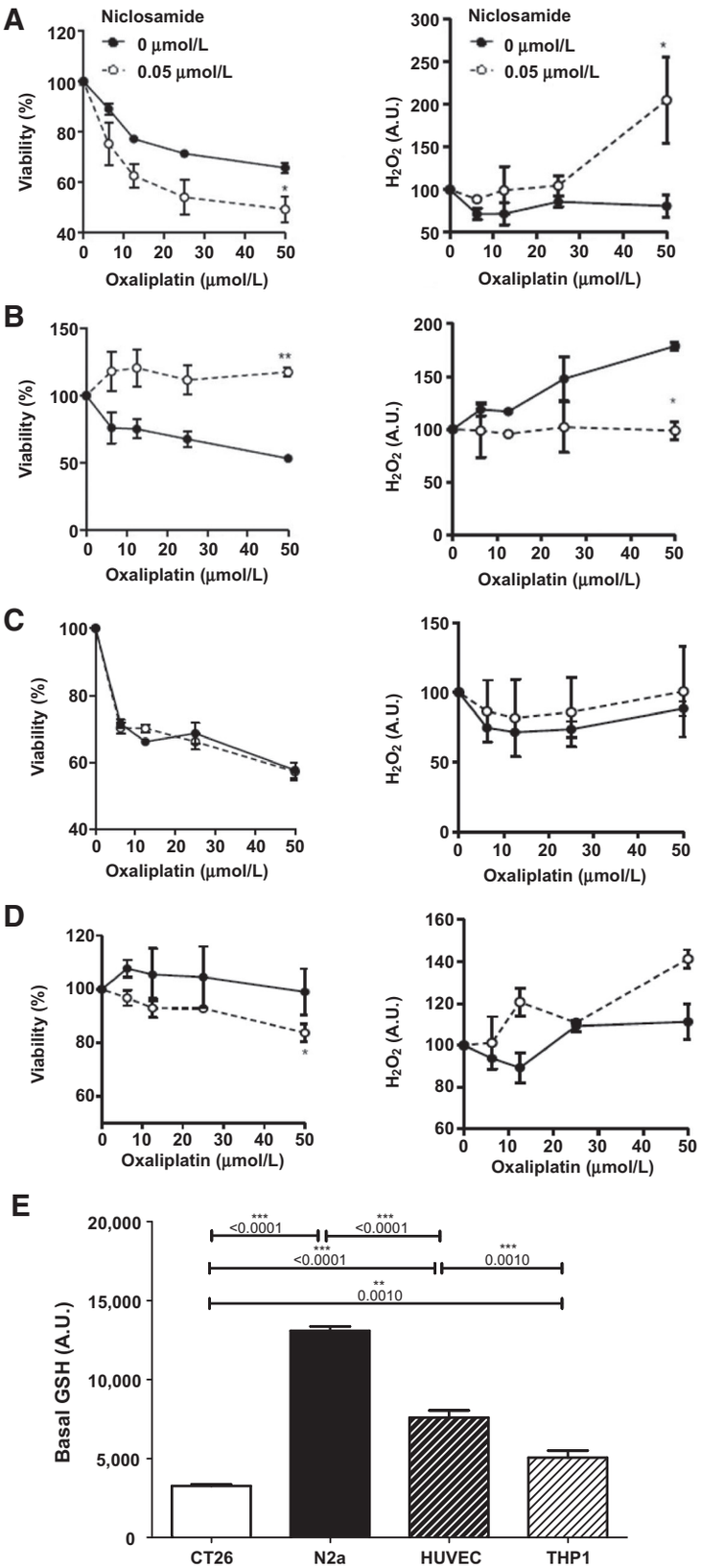

Figure 1.
In vitro effects of oxaliplatin associated or not with niclosamide on viability and oxaliplatin-induced ROS production. **A,** CT26 cells. **B,** N2a cells. **C,** HUVEC. **D,** THP1 cells. Viability was expressed as percent ± SD versus cells in culture medium alone (100% viability). **E,** Reduced GSH was also assessed under normal cell culture growth conditions with monochlorobimane. Data from at least three independent experiments have been pooled and were expressed as means ± SD of triplicates. *, $P < 0.05$; **, $P < 0.01$ versus oxaliplatin.

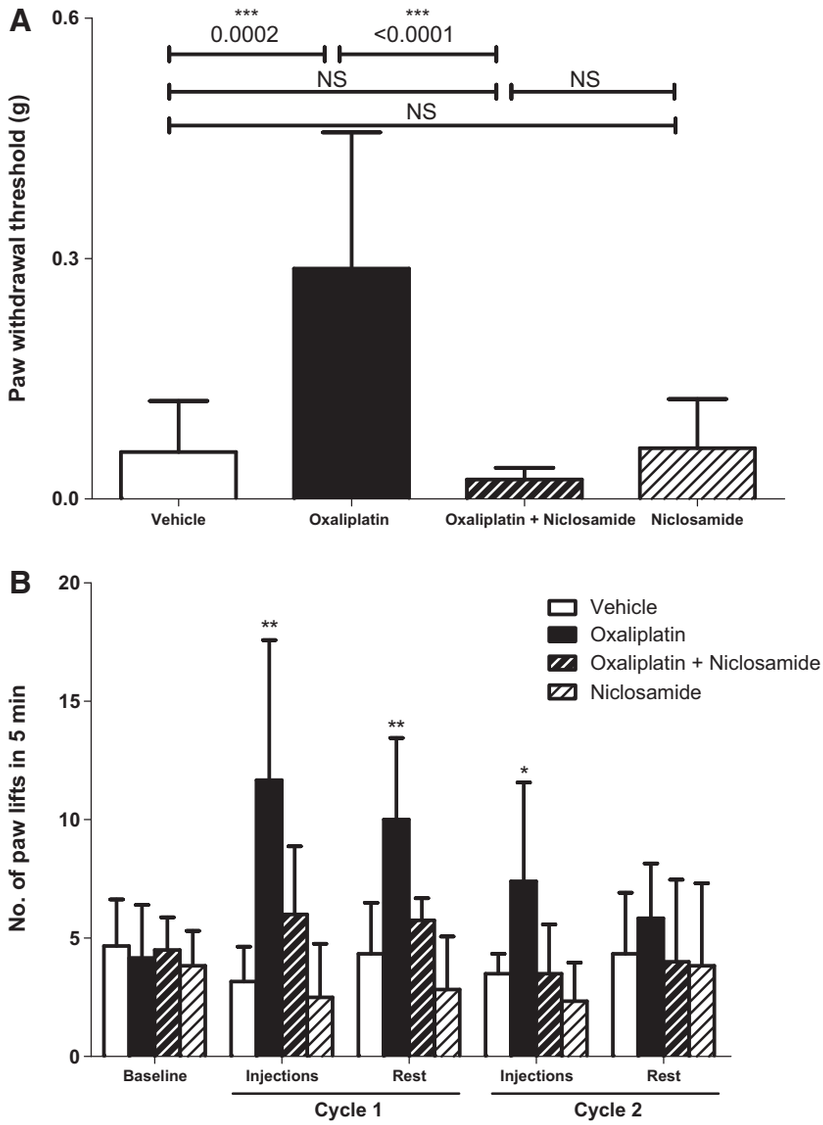

Figure 2.

In vivo effects of oxaliplatin and niclosamide on mouse tactile sensitivity and cold hyperalgesia. **A,** Experimental mice received oxaliplatin (10 mg/kg) weekly and niclosamide (10 mg/kg) three times a week for 8 weeks. NS, not significant. Control mice received either oxaliplatin or vehicle alone. Nociception was evaluated using a von Frey test at 4 weeks. **B,** Evaluation of hyperalgesia required two 5-day cycles of daily oxaliplatin (3 mg/kg). Control mice received either oxaliplatin or vehicle alone. Cold hyperalgesia was evaluated using a cold plate set at +2°C. Data are expressed as the means ± SD of 13 and 6 different mice under each condition for the von Frey test and the cold plate test, respectively. NS, nonsignificant. *, $P < 0.05$; **, $P < 0.01$ versus vehicle or oxaliplatin.

The oxaliplatin-induced sensory and motor alterations were not detected in mice injected with oxaliplatin plus niclosamide or niclosamide alone (Fig. 3; Supplementary Fig. S1; Supplementary Table S1). These observations further validate niclosamide as a potentially neuroprotective molecule, as they highlighted the maintenance of the peripheral nervous system functioning by the teniacide.

The morphology of myelinated axons of mouse sciatic nerves was examined using confocal microscopy (Fig. 4). Quantification of morphometric parameters of single myelinated axons revealed a significant increase in the nodal diameter, length, and volume, as functions of the internodal diameter, in mice injected for 5 weeks with oxaliplatin, compared with vehicle-treated animals (Fig. 4B, left; Supplementary Table S2). These results are likely the consequence of oxaliplatin-induced membrane hyperexcitability. In these animals, a reduction in the internodal diameter was also observed, which may reflect either a preferential loss of large myelinated nerve fibers or an alteration in myelin sheath layers surrounding the axons. These morphometric parameters were not altered in mice injected for 5 weeks with oxaliplatin plus niclosamide (Fig. 4B, middle; Supplementary Table S2) or niclosamide alone (Fig. 4B, right; Supplementary Table S2). Therefore, oxaliplatin induced a mixed form of peripheral neuropathy, with both the myelin sheath being thinner and the axons being swollen as indicated by the increase in the nodal diameter. Niclosamide addressed both of these parameters, which may account for its efficacy in maintaining nervous functioning of the peripheral nervous system in oxaliplatin-treated mice.

The density of intraepidermal nerve fibers was examined in the paws of mice injected with vehicle, oxaliplatin, oxaliplatin plus niclosamide, or niclosamide alone for 8 weeks. Staining of the nerve fibers with PGP9.5 antibody revealed a reduced intraepidermal nerve fiber density in the paw skin of oxaliplatin mice (Fig. 5A). Niclosamide abrogated this alteration in oxaliplatin mice and maintained density of PGP9.5-stained nerves in mice that had also been treated with oxaliplatin (Fig. 5B).

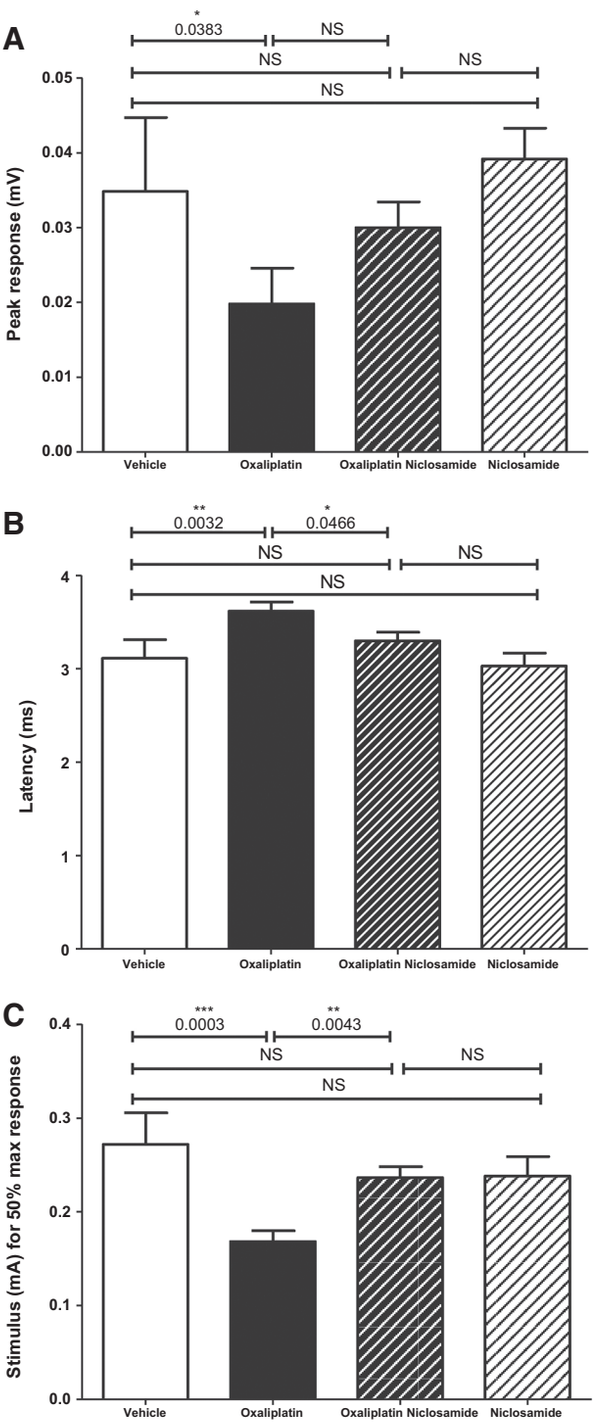

Figure 3.

In vivo effects of oxaliplatin and niclosamide on mouse sensory excitability. **A,** Mean values ± SD of maximal CNAP amplitude, that is, peak amplitude. NS, not significant. **B,** Latency. **C,** Stimulus intensity to evoke 50% of maximal CNAP amplitude, that is, stimulus (mA) for 50% maximal response recorded from the tail base in response to caudal nerve stimulation of mice treated for 5 weeks with vehicle ($n = 6$), oxaliplatin ($n = 5$), oxaliplatin plus niclosamide ($n = 5$), or niclosamide alone ($n = 6$). Note the absence of effect of oxaliplatin plus niclosamide and niclosamide alone on these three parameters versus vehicle.

The myelin content of sciatic nerves from experimental and control groups of mice was also assessed. Analyses of myelin content revealed a demyelination in oxaliplatin-treated mice compared with animals injected with vehicle, oxaliplatin plus niclosamide, or niclosamide alone (Fig. 5C). Staining of the nerves with Luxol allowed the quantification of the demyelination in sciatic nerves from oxaliplatin mice (Fig. 5D). Niclosamide abrogated the reduction in myelin sheath thickness observed in oxaliplatin mice, which translated in either partial or total degradation of the myelin sheath surrounding the axons of neuropathic mice and higher G-ratios (Fig. 5D).

Results obtained from the neurologic tests provided a rationale for the use of niclosamide as a neuroprotective drug, but further data regarding its effect on oxaliplatin efficacy had to be gathered to guarantee its safety in addressing the primary aspect of the condition, which is tumor growth. From the 11th day of treatment on, mice treated with niclosamide alone had smaller tumors than nontreated mice (2,083 ± 229.1 mm^3 with niclosamide vs. 2,819 ± 173.0 mm^3 with vehicle). Niclosamide maintained oxaliplatin efficacy, as mice treated from day 4 on with oxaliplatin plus niclosamide had, from day 4, smaller tumors than mice treated with vehicle (at day 4, 253.5 ± 30.01 mm^2 with oxaliplatin plus niclosamide vs. 782.0 ± 98.54 mm^3 with vehicle, and at day 21, 1,167 ± 182.9 mm^3 with oxaliplatin plus niclosamide vs. 9,001 ± 448.8 mm^3 with vehicle; Fig. 6A). Oxaliplatin plus niclosamide-treated mice had similar tumor sizes than oxaliplatin-treated mice at 3 weeks (1,167 ± 182.9 mm^3 with oxaliplatin plus niclosamide vs. 1,127 ± 186.0 mm^3 with oxaliplatin alone; Fig. 6A).

To evaluate the systemic effects of niclosamide on proinflammatory cytokine levels, serum samples were analyzed. Serum IL6 levels were significantly increased in the oxaliplatin group of mice compared with the oxaliplatin plus niclosamide, vehicle, and niclosamide groups (4.812 ± 1.299 ng/mL with oxaliplatin vs. 1.064 ± 0.943 ng/mL with oxaliplatin plus niclosamide, vs. vehicle 1.477 ± 0.451 ng/mL, and vs. niclosamide 1.631 ± 0.647 ng/mL; Fig. 6B). Serum TNFα levels were also significantly increased in the oxaliplatin group compared with all other groups of mice (0.9076 ± 0.3155 pg/mL with oxaliplatin vs. 0.1273 ± 0.1127 pg/mL with oxaliplatin plus niclosamide, vs. vehicle 0.1436 ± 0.0553 pg/mL, and vs. niclosamide 0.0822 ± 0.0689 pg/mL; Fig. 6C). Serum AOPPs were also found to be significantly increased in mice receiving only oxaliplatin compared with the other experimental mice groups (0.1040 ± 0.01885 μmol/L with oxaliplatin vs. 0.05587 ± 0.006318 μmol/L with oxaliplatin plus niclosamide, vs. vehicle 0.05180 ± 0.006046 μmol/L, and vs. niclosamide 0.05057 ± 0.008539 μmol/L; Fig. 6D).

Discussion

This report evidences the beneficial effects of niclosamide on oxaliplatin-induced peripheral neuropathies, muscle cramps, and tumor growth. Niclosamide protects neuron-like cells while potentiating the cytotoxic effects of the chemotherapy on cancer cells. Thus, *in vivo*, this molecule prevents oxaliplatin-induced peripheral neuropathies without impairing chemotherapy efficacy. To test our hypothesis that niclosamide is effective in preventing both forms of peripheral neuropathy induced by oxaliplatin, we used a murine model described previously (1).

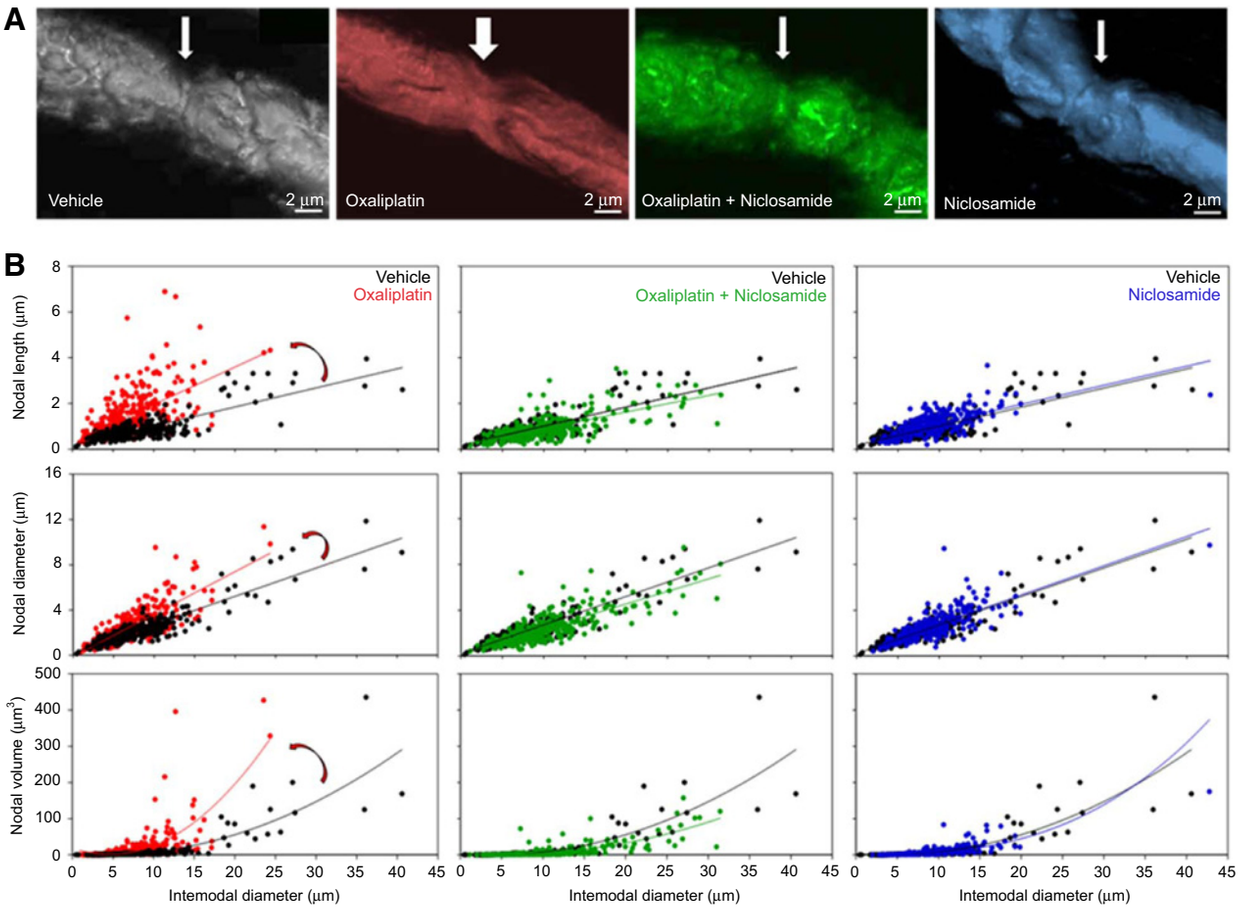

Figure 4.

Effects of oxaliplatin and niclosamide on the morphology of single myelinated axons isolated from mouse sciatic nerves. **A,** Mice ($n = 4$ in each group) were injected with vehicle, oxaliplatin, oxaliplatin plus niclosamide, or niclosamide alone, for 5 weeks. Typical images of single myelinated axons, stained with FM1-43, acquired under each condition using confocal microscopy. The arrows indicate the node of Ranvier and are proportional to its size. **B,** Representations of nodal length, diameter, and volume, as functions of internodal diameter, of myelinated axons isolated from mice injected with vehicle (black closed circles, $n = 305$), oxaliplatin (red closed circles, $n = 319$), oxaliplatin plus niclosamide (green closed circles, $n = 314$), or niclosamide alone (blue closed circles, $n = 271$). The curves represent the linear (top and middle) or nonlinear (bottom) fits of data points with R^2 (correlation coefficients) between 0.663 and 0.824. Left, arrows underline the effects of oxaliplatin.

Our results show that neuron-like cells retain their integrity when exposed to oxaliplatin if associated with niclosamide. These cells produce reduced levels of H_2O_2 compared with cells exposed to oxaliplatin alone. Furthermore, niclosamide also potentiates the cytotoxic effect of oxaliplatin on tumor cells via an increase in H_2O_2 production. These findings are of prime interest as ROS are key mediators of oxaliplatin-induced neuron cytotoxicity (26). In addition, tumor growth can also be regulated by modulating the production of ROS (10). The differences in ROS production between cell types exposed to niclosamide could be related to basal levels of GSH (33). Interestingly, we and others have shown that normal cells and tumor cells respond differently to H_2O_2-induced cell death due to differences in basal H_2O_2 levels and antioxidant defense systems between cell types (10, 34, 35). Tumor cells are more sensitive to ROS-induced cell death than normal cells due to increased metabolism of tumor cells and antioxidant defense exhaustion. Interestingly, in normal cells, similar levels that kill tumor cells favor cellular viability and proliferation through adaptation and mobilization of antioxidant defenses, usually through NRF2 induction (36, 37). Furthermore, GSH homeostasis is of prime importance for neurons as their depletion in this antioxidant molecule ultimately leads to their senescence mediated by oxidative stress (38). Several studies concur with the observation that GSH-mediated detoxification of H_2O_2 is paramount to address neurologic disorders, may they be central or peripheral (39, 40). In clinical settings, GSH infusions significantly reduced the severity of the neurodegenerative side effects of oxaliplatin (41). These results prompted us to investigate *in vivo* the effects of niclosamide on oxaliplatin-treated mice.

A diminished nociception was observed i*n vivo* in oxaliplatin mice. This impairment was abrogated by associating niclosamide to the chemotherapy. This finding can be linked with data gained from immunohistochemical studies that revealed reduced intraepidermal nerve fiber density in mice treated with

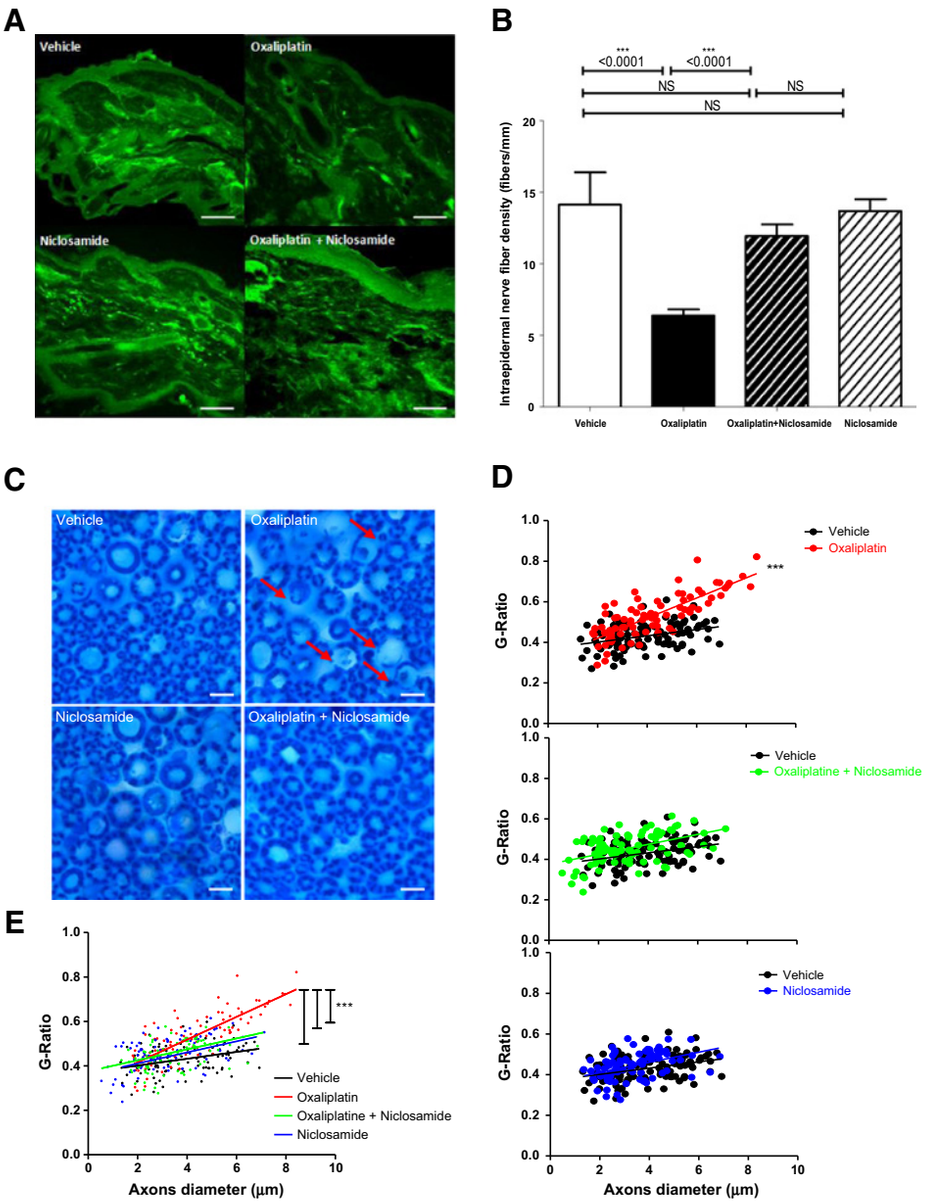

Figure 5.
Characterization Of Cutaneous Nerve Fiber Density By PGP9.5 Staining And Paraffin-Included Luxol® Blue Fast (Myelin)-Treated Transversal 8 µm Sections Of Sciatic Nerves From Mice. **A,** Staining with PGP9.5 of cutaneous nerve fibers. **B,** Analysis of intraepidermal nerve fiber density from paw skin samples (6 µm) mice treated for 8 weeks with vehicle, oxaliplatin, oxaliplatin plus niclosamide or niclosamide as determined by a masked pathologist using a two-tailed Student's *t* test. ***, $P < 0.001$ *versus* oxaliplatin. Error bars represent standard deviation of the mean. Magnification ×40. Scale bars, 100 µm. **C,** Histological staining of peripheral myelin with Luxol® Blue Fast. **D,** Analysis of myelin content as determined by a masked pathologist using a two-tailed Student's *t* test. ***, $P < 0.001$ *versus* oxaliplatin. **E,** Compiled analysis of myelin content. Error bars represent standard deviation of the mean. A two-tailed Student's *t* test was performed. ***, $P < 0.001$ *versus* oxaliplatin. Magnification ×100. Scale bars, 2 µm.

oxaliplatin (42, 43). Niclosamide permits the maintenance of the density of these fibers in oxaliplatin mice. It is possible that niclosamide protects these fibers by limiting local inflammation mediated by the activation of Langerhans cells and astrocytes (44) and oxidative species. ROS production and inflammation has been linked to the etiology of peripheral neuropathies (45). ROS may not only act locally but also favor a state of sensitization to pain through spinal mechanisms, namely at the dorsal horn region, resulting in centrally lowered pain thresholds (46). These findings were furthered explained through the use of ROS scavenger molecules, which reduced the development of both thermoalgesia but also mechanically triggered pain in a murine model of neuropathic pain (47). Cold hyperalgesia induced by oxaliplatin treatment is abrogated by niclosamide. Thermoception is achieved through two different types of nerve fibers: A delta-type nerve fibers and C-type nerve fibers. Unlike C nerve fibers, A delta nerve fibers are myelinated and convey action potentials of high speed. Niclosamide could act on morphologic properties of myelinated fibers while maintaining functional properties of larger fibers conveying slower action potentials.

Electrophysiologic sensory and motor recordings from the mouse, *in vivo*, reveal oxaliplatin-induced functional impairment that consists in a global membrane hyperexcitability state, including, in particular, reduced stimulus intensity to evoke 50% of maximal CNAP or CMAP amplitude, and lower axonal accommodation capacities to hyperpolarizations, without any change in resting membrane potential. This functional impairment translates apparent reduction in the number of fast-conducting sensory fibers and modifications in the density and/or functioning of transitory sodium channels, inward rectifier, and fast potassium channels, as well as cyclic nucleotide-gated channels, those of

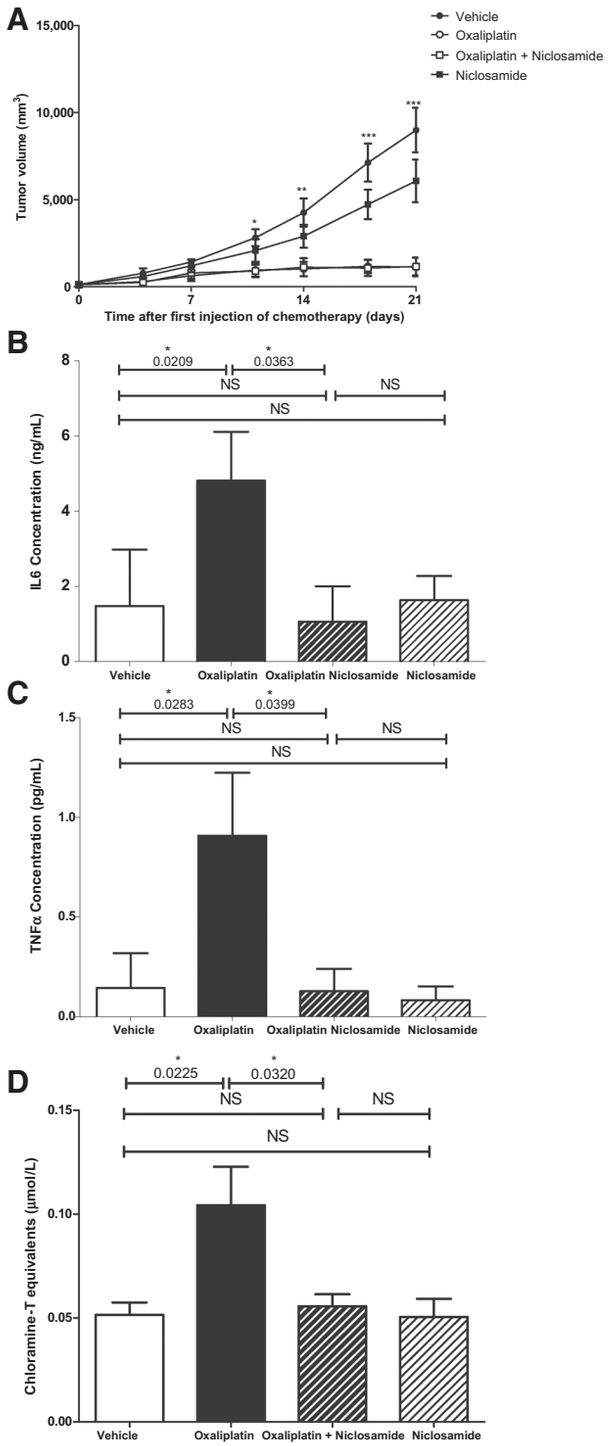

Figure 6.

Evaluation of oxaliplatin efficacy in combination with niclosamide in a tumor growth model. **A,** Tumor size in mice injected subcutaneously into the back with 10^6 CT26 cells and treated with vehicle, oxaliplatin, oxaliplatin associated with niclosamide, or niclosamide alone. **B,** Mean values ± SD of tumor volumes under each condition. *, $P < 0.05$; **, $P < 0.01$; ***, $P < 0.001$ versus vehicle. ELISA-quantified levels of IL6 in sera from mice treated for 4 weeks with vehicle, oxaliplatin, oxaliplatin associated with niclosamide, or niclosamide alone. NS, not significant. **C,** ELISA-quantified levels of TNFα in sera from mice treated for 4 weeks with vehicle, oxaliplatin, oxaliplatin associated with niclosamide, or niclosamide alone. **D,** AOPPs levels in sera from mice treated for 4 weeks with vehicle, oxaliplatin, oxaliplatin associated with niclosamide, or niclosamide alone. Data, means ± SD. *, $P < 0.05$, versus vehicle or oxaliplatin.

persistent sodium and slow potassium channels being unaffected. This state can be triggered by oxaliplatin infusion and has been linked to demyelination (48). However, impairment of voltage-gated channel functioning has been widely documented as implicated in the etiology of oxaliplatin-induced peripheral neuropathies (49). Previous reports highlight this peculiar relation between demyelination and hyperexcitability and attribute this to a proximal compensatory burst of nerve influx (50). Hyperexcitability, by allowing sodium influx, produces an increase in internal sodium concentration compensated by an influx of water, which enhances the nodal volume (51) similarly to a demyelination process. This maladaptive process was coined "homeostatic plasticity" (52). Interestingly, the sensory and motor alterations of the mouse produced by the antitumor agent were not detected in mice injected with oxaliplatin plus niclosamide or niclosamide alone.

Various studies correlate impairment of tactile perception and altered thermoception in rodents presenting peripheral neuropathies with intraepidermal nerve fiber loss (42). Mice that present altered neurologic properties display profoundly altered cutaneous innervations in terms of both morphology and density. Morphologic analyses of sciatic nerves reveal a decreased myelin sheath thickness as well as complete destruction of the myelin sheath in some areas around the axons from sciatic nerves of oxaliplatin-treated mice. This degradation and reduction in thickness of the myelin sheath is prevented by niclosamide. Niclosamide may be able to address channelopathies by diminishing the extent of the demyelination observed in mice receiving the chemotherapy alone through the modulation of the activity of glial cells in the immediate surroundings of pathogenic nerve fibers.

Markers of inflammation, IL6 and TNFα levels, were significantly reduced by niclosamide in sera of mice treated with oxaliplatin. The production of inflammatory cytokines can induce peripheral neuropathies in rodent models (53) and is increased in patients suffering from these neurologic disorders (54), thus further explaining the neuroprotection conferred to oxaliplatin-treated mice receiving the teniacide niclosamide. Studies pinpointing the involvement of several proinflammatory cytokines in the development of neuropathic pain prompted neuroimmunity to be extensively investigated over recent years (29, 55). These observations led to increased interest in molecules, allowing the downregulation or complete blockage of the expression of these neuropathy-associated cytokines (56–58). Despite these efforts, to date, there is no molecule indicated specifically for the treatment of neuropathic pain. Niclosamide, by limiting systemic inflammation through the prevention of the burst in oxidative stress induced by oxaliplatin and mediated by H_2O_2, could prevent the impairment of myelin generation and allow undisrupted nervous conduction across the peripheral nervous system. Our study demonstrates that niclosamide increases the therapeutic index of oxaliplatin by both reducing the neurodegenerative side effects of oxaliplatin and enhancing the cytotoxic effects of this chemotherapy on cancer cells. The absence of potentiation

of oxaliplatin *in vivo* is most likely linked to oxaliplatin's inherent antitumor activity being at this dosage (10 mg/kg) sufficient to cause tumor cell death.

Further investigations focusing on potential neuroprotection by niclosamide could shed light on the benefit that patients could gain from receiving this well-tolerated teniacide in association with other treatments currently available to address axonal, demyelinating, or mixed peripheral neuropathies of various etiologies.

Disclosure of Potential Conflicts of Interest

No potential conflicts of interest were disclosed.

Authors' Contributions

Conception and design: O. Cerles, R. Coriat, F. Batteux, C. Nicco
Development of methodology: O. Cerles, M.-A. Guillaumot, R. Coriat, N. Kavian, F. Batteux, C. Nicco
Acquisition of data (provided animals, acquired and managed patients, provided facilities, etc.): O. Cerles, E. Benoit, C. Chéreau, S. Chouzenoux, F. Morin, M.-A. Guillaumot, R. Coriat, T. Loussier, L. Marcellin, C. Nicco
Analysis and interpretation of data (e.g., statistical analysis, biostatistics, computational analysis): O. Cerles, E. Benoit, C. Chéreau, S. Chouzenoux, M.-A. Guillaumot, R. Coriat, N.E.B. Saidu, F. Batteux, C. Nicco
Writing, review, and/or revision of the manuscript: O. Cerles, E. Benoit, S. Chouzenoux, M.-A. Guillaumot, R. Coriat, P. Santulli, N.E.B. Saidu, B. Weill, F. Batteux, C. Nicco
Administrative, technical, or material support (i.e., reporting or organizing data, constructing databases): C. Chéreau, R. Coriat, N. Kavian, C. Nicco
Study supervision: F. Batteux, C. Nicco

Acknowledgments

The authors are grateful to Agnes Colle for her excellent typing of the manuscript.

Grant Support

This study was supported by Institut National de la Santé et de la Recherche Médicale (INSERM) grants that were distributed by Institut Cochin (to F. Batteux).

The costs of publication of this article were defrayed in part by the payment of page charges. This article must therefore be hereby marked *advertisement* in accordance with 18 U.S.C. Section 1734 solely to indicate this fact.

Received May 20, 2016; revised October 21, 2016; accepted November 17, 2016; published OnlineFirst December 15, 2016.

References

1. Coriat R, Alexandre J, Nicco C, Quinquis L, Benoit E, Chéreau C, et al. Treatment of oxaliplatin-induced peripheral neuropathy by intravenous mangafodipir. J Clin Invest 2014;124:262–72.
2. Masuda H, Tanaka T, Takahama U. Cisplatin generates superoxide anion by interaction with DNA in a cell-free system. Biochem Biophys Res Commun 1994;203:1175–80.
3. Raymond E, Faivre S, Woynarowski JM, Chaney SG. Oxaliplatin: mechanism of action and antineoplastic activity. Semin Oncol 1998;25:4–12.
4. Canta A, Pozzi E, Carozzi VA. Mitochondrial dysfunction in chemotherapy-induced peripheral neuropathy (CIPN) toxics2015;3:198–223.
5. Egashira N, Hirakawa S, Kawashiri T, Yano T, Ikesue H, Oishi R. Mexiletine reverses oxaliplatin-induced neuropathic pain in rats. J Pharmacol Sci 2010;112:473–6.
6. Adelsberger H, Quasthoff S, Grosskreutz J, Lepier A, Eckel F, Lersch C. The chemotherapeutic oxaliplatin alters voltage-gated Na(+) channel kinetics on rat sensory neurons. Eur J Pharmacol 2000;406:25–32.
7. Kagiava A, Tsingotjidou A, Emmanouilides C, Theophilidis G. The effects of oxaliplatin, an anticancer drug, on potassium channels of the peripheral myelinated nerve fibres of the adult rat. Neurotoxicology 2008;29:1100–6.
8. Schulze C, McGowan M, Jordt SE, Ehrlich BE. Prolonged oxaliplatin exposure alters intracellular calcium signaling: a new mechanism to explain oxaliplatin-associated peripheral neuropathy. Clin Colorectal Cancer 2011;10:126–33.
9. Siau C, Bennett GJ. Dysregulation of cellular calcium homeostasis in chemotherapy-evoked painful peripheral neuropathy. Anesth Analg 2006; 102:1485–90.
10. Laurent A, Nicco C, Chéreau C, Goulvestre C, Alexandre J, Alves A, et al. Controlling tumor growth by modulating endogenous production of reactive oxygen species. Cancer Res 2005;65:948–56.
11. Gamelin E, Gamelin L, Bossi L, Quasthoff S. Clinical aspects and molecular basis of oxaliplatin neurotoxicity: current management and development of preventive measures. Semin Oncol 2002;29:21–33.
12. Carozzi VA, Marmiroli P, Cavaletti G. The role of oxidative stress and antioxidant treatment in platinum-induced peripheral neurotoxicity. Curr Cancer Drug Targets 2010;10:670–82.
13. Carozzi VA, Canta A, Chiorazzi A. Chemotherapy-induced peripheral neuropathy: what do we know about mechanisms? Neurosci Lett 2015;596:90–107.
14. Nassini R, Gees M, Harrison S, De Siena G, Materazzi S, Moretto N, et al. Oxaliplatin elicits mechanical and cold allodynia in rodents via TRPA1 receptor stimulation. Pain 2011;152:1621–31.
15. Lim SC, Choi JE, Kang HS, Han SI. Ursodeoxycholic acid switches oxaliplatin-induced necrosis to apoptosis by inhibiting reactive oxygen species production and activating p53-caspase 8 pathway in HepG2 hepatocellular carcinoma. Int J Cancer 2010;126:1582–95.
16. Joseph EK, Chen X, Bogen O, Levine JD. Oxaliplatin acts on IB4-positive nociceptors to induce an oxidative stress-dependent acute painful peripheral neuropathy. J Pain 2008;9:463–72.
17. Zheng H, Xiao WH, Bennett GJ. Functional deficits in peripheral nerve mitochondria in rats with paclitaxel- and oxaliplatin-evoked painful peripheral neuropathy. Exp Neurol 2011;232:154–61.
18. Extra JM, Marty M, Brienza S, Misset JL. Pharmacokinetics and safety profile of oxaliplatin. Semin Oncol 1998;25:13–22.
19. Hartmann JT, Lipp HP. Toxicity of platinum compounds. Expert Opin Pharmacother 2003;4:889–901.
20. Li Y, Li PK, Roberts MJ, Arend RC, Samant RS, Buchsbaum DJ. Multi-targeted therapy of cancer by niclosamide: a new application for an old drug. Cancer Lett 2014;349:8–14.
21. You S, Li R, Park D, Xie M, Sica GL, Cao Y, et al. Disruption of STAT3 by niclosamide reverses radioresistance of human lung cancer. Mol Cancer Ther 2014;13:606–16.
22. Lee SL, Son AR, Ahn J, Song JY. Niclosamide enhances ROS-mediated cell death through c-Jun activation. Biomed Pharmacother 2014; 68:619–24.
23. Toyama S, Shimoyama N, Ishida Y, Koyasu T, Szeto HH, Shimoyama M. Characterization of acute and chronic neuropathies induced by oxaliplatin in mice and differential effects of a novel mitochondria-targeted antioxidant on the neuropathies. Anesthesiology 2014;120:459–73.
24. Miraucourt LS, Moisset X, Dallel R, Voisin DL. Glycine inhibitory dysfunction induces a selectively dynamic, morphine-resistant, and neurokinin 1 receptor- independent mechanical allodynia. J Neurosci 2009;29:2519–27.
25. Ta LE, Low PA, Windebank AJ. Mice with cisplatin and oxaliplatin-induced painful neuropathy develop distinct early responses to thermal stimuli. Mol Pain 2009;5:9.
26. Areti A, Yerra VG, Naidu V, Kumar A. Oxidative stress and nerve damage: role in chemotherapy induced peripheral neuropathy. Redox Biol 2014;2:289–95.
27. Kiernan MC, Burke D, Andersen KV, Bostock H. Multiple measures of axonal excitability: a new approach in clinical testing. Muscle Nerve 2000;23:399–409.
28. Krishnan AV, Lin CS, Park SB, Kiernan MC. Assessment of nerve excitability in toxic and metabolic neuropathies. J Peripher Nerv Syst 2008;13:7–26.

29. Austin PJ, Moalem-Taylor G. The neuro-immune balance in neuropathic pain: involvement of inflammatory immune cells, immune-like glial cells and cytokines. J Neuroimmunol 2010;229:26–50.
30. Preitschopf A, Li K, Schorghofer D, Kinslechner K, Schutz B, Thi Thanh Pham H, et al. mTORC1 is essential for early steps during Schwann cell differentiation of amniotic fluid stem cells and regulates lipogenic gene expression. PLoS One 2014;9:e107004.
31. Shen YA, Chen Y, Dao DQ, Mayoral SR, Wu L, Meijer D, et al. Phosphorylation of LKB1/Par-4 establishes Schwann cell polarity to initiate and control myelin extent. Nat Commun 2014;5:4991.
32. Zhang CJ, Zhai H, Yan Y, Hao J, Li MS, Jin WN, et al. Glatiramer acetate ameliorates experimental autoimmune neuritis. Immunol Cell Biol 2014;92:164–9.
33. Morales MC, Perez-Yarza G, Nieto-Rementeria N, Boyano MD, Jangi M, Atencia R, et al. Intracellular glutathione levels determine cell sensitivity to apoptosis induced by the antineoplasic agent N-(4-hydroxyphenyl) retinamide. Anticancer Res 2005;25:1945–51.
34. Alexandre J, Nicco C, Chéreau C, Laurent A, Weill B, Goldwasser F, et al. Improvement of the therapeutic index of anticancer drugs by the superoxide dismutase mimic mangafodipir. J Natl Cancer Inst 2006;98:236–44.
35. Trachootham D, Alexandre J, Huang P. Targeting cancer cells by ROS-mediated mechanisms: a radical therapeutic approach? Nat Rev Drug Discov 2009;8:579–91.
36. Gallorini M, Petzel C, Bolay C, Hiller KA, Cataldi A, Buchalla W, et al. Activation of the Nrf2-regulated antioxidant cell response inhibits HEMA-induced oxidative stress and supports cell viability. Biomaterials 2015; 56:114–28.
37. Gonzalez-Reyes S, Guzman-Beltran S, Medina-Campos ON, Pedraza-Chaverri J. Curcumin pretreatment induces Nrf2 and an antioxidant response and prevents hemin-induced toxicity in primary cultures of cerebellar granule neurons of rats. Oxid Med Cell Longev 2013;2013:801418.
38. Belrose JC, Xie YF, Gierszewski LJ, MacDonald JF, Jackson MF. Loss of glutathione homeostasis associated with neuronal senescence facilitates TRPM2 channel activation in cultured hippocampal pyramidal neurons. Mol Brain 2012;5:11.
39. Bains JS, Shaw CA. Neurodegenerative disorders in humans: the role of glutathione in oxidative stress-mediated neuronal death. Brain Res Brain Res Rev 1997;25:335–58.
40. Sagara M, Satoh J, Wada R, Yagihashi S, Takahashi K, Fukuzawa M, et al. Inhibition of development of peripheral neuropathy in streptozotocin-induced diabetic rats with N-acetylcysteine. Diabetologia 1996;39:263–9.
41. Cascinu S, Catalano V, Cordella L, Labianca R, Giordani P, Baldelli AM, et al. Neuroprotective effect of reduced glutathione on oxaliplatin-based chemotherapy in advanced colorectal cancer: a randomized, double-blind, placebo-controlled trial. J Clin Oncol 2002;20:3478–83.
42. Boyette-Davis J, Dougherty PM. Protection against oxaliplatin-induced mechanical hyperalgesia and intraepidermal nerve fiber loss by minocycline. Exp Neurol 2011;229:353–7.
43. Xiao WH, Zheng H, Bennett GJ. Characterization of oxaliplatin-induced chronic painful peripheral neuropathy in the rat and comparison with the neuropathy induced by paclitaxel. Neuroscience 2012;203:194–206.
44. Di Cesare Mannelli L, Pacini A, Micheli L, Tani A, Zanardelli M, Ghelardini C. Glial role in oxaliplatin-induced neuropathic pain. Exp Neurol 2014;261:22–33.
45. Low PA, Nickander KK, Tritschler HJ. The roles of oxidative stress and antioxidant treatment in experimental diabetic neuropathy. Diabetes 1997;46:38–42.
46. Gao X, Kim HK, Chung JM, Chung K. Reactive oxygen species (ROS) are involved in enhancement of NMDA-receptor phosphorylation in animal models of pain. Pain 2007;131:262–71.
47. Siniscalco D, Fuccio C, Giordano C, Ferraraccio F, Palazzo E, Luongo L, et al. Role of reactive oxygen species and spinal cord apoptotic genes in the development of neuropathic pain. Pharmacol Res 2007;55:158–66.
48. Hamada MS, Kole MH. Myelin loss and axonal ion channel adaptations associated with gray matter neuronal hyperexcitability. J Neurosci 2015;35:7272–86.
49. Wilson RH, Lehky T, Thomas RR, Quinn MG, Floeter MK, Grem JL. Acute oxaliplatin-induced peripheral nerve hyperexcitability. J Clin Oncol 2002;20:1767–74.
50. Smith KJ, Hall SM. Factors directly affecting impulse transmission in inflammatory demyelinating disease: recent advances in our understanding. Curr Opin Neurol 2001;14:289–98.
51. Mattei C, Molgo J, Benoit E. Involvement of both sodium influx and potassium efflux in ciguatoxin-induced nodal swelling of frog myelinated axons. Neuropharmacology 2014;85:417–26.
52. Wang G, Thompson SM. Maladaptive homeostatic plasticity in a rodent model of central pain syndrome: thalamic hyperexcitability after spinothalamic tract lesions. J Neurosci 2008;28:11959–69.
53. Cunha TM, Verri WA Jr, Silva JS, Poole S, Cunha FQ, Ferreira SH. A cascade of cytokines mediates mechanical inflammatory hypernociception in mice. Proc Natl Acad Sci U S A 2005;102:1755–60.
54. Uceyler N, Rogausch JP, Toyka KV, Sommer C. Differential expression of cytokines in painful and painless neuropathies. Neurology 2007; 69:42–9.
55. Tian L, Ma L, Kaarela T, Li Z. Neuroimmune crosstalk in the central nervous system and its significance for neurological diseases. J Neuroinflammation 2012;9:155.
56. Guptarak J, Wanchoo S, Durham-Lee J, Wu Y, Zivadinovic D, Paulucci-Holthauzen A, et al. Inhibition of IL-6 signaling: A novel therapeutic approach to treating spinal cord injury pain. Pain 2013; 154:1115–28.
57. Iwatsuki K, Arai T, Ota H, Kato S, Natsume T, Kurimoto S, et al. Targeting anti-inflammatory treatment can ameliorate injury-induced neuropathic pain. PLoS One 2013;8:e57721.
58. Shi X, Chen Y, Nadeem L, Xu G. Beneficial effect of TNF-α inhibition on diabetic peripheral neuropathy. J Neuroinflammation 2013;10:69.